

# Chapter 2

## Enzyme-Based Reversible Logic Gates Operated in Flow Cells

Evgeny Katz and Brian E. Fratto

**Abstract** Reversible logic gates, such as Feynman gate (Controlled NOT), Double Feynman gate, Toffoli gate and Peres gate, with 2-input/2-output and 3-input/3-output channels, were realized using reactions biocatalyzed by enzymes and performed in flow systems. The flow devices were constructed using a modular approach, where each flow cell was modified with one enzyme that biocatalyzed one chemical reaction. Assembling the biocatalytic flow cells in different networks, with different pathways for transporting the reacting species, allowed the multi-step processes mimicking various reversible logic gates. The chapter emphasizes “logic” reversibility but not the “physical” reversibility of the constructed systems. Their advantages and disadvantages are discussed and potential use in biosensing systems, rather than in computing devices, is suggested.

### 2.1 Introduction

Computer technology presently based on silicon-materials and binary algorithms is coming to the end of its exponential development, being limited not only by further component-miniaturization but also the speed of their operation. Conceptually novel ideas are needed to break through these limitations. In order to reach another level of information processing and to maintain fast progress in computer technology, new and intuitive forms of technology are needed. The quest for novel ideas in information processing has resulted in several exciting directions in the general area of unconventional computing [1], including research in quantum computing and biologically inspired molecular computing. While molecular computing [2–4] is generally motivated by mimicking natural biological information processing, the tools are not necessary based on biological systems and often represented by synthetic molecules with signal-controlled properties. Synthetic molecular systems [5] and nano-species [6] have been designed to mimic the operation of Boolean logic gates and demon-

---

E. Katz (✉) · B.E. Fratto  
Clarkson University, Potsdam, NY, USA  
e-mail: ekatz@clarkson.edu

strate basic arithmetic functions and memory units. Despite the great progress that has been achieved in the development of molecular computing systems [7, 8], the major challenge in this research area is further increase of their complexity [9]. A new advancement in the development of molecular information systems has been achieved with use of biomolecular species [10, 11], borrowing some ideas from systems biology [12]. The first demonstration of computational processes performed by DNA molecules to solve some combinatorial problems [13] was recently extended to include the use of various biomolecular systems based on DNA/RNA [14–16], oligopeptides [17], proteins [18], enzymes [19] and even whole biological cells [20, 21] for mimicking various information processing steps, Fig. 2.1. One of the obvious advantages of biomolecular systems is their ability to integrate in artificially designed complex reacting processes mimicking multi-step information processing networks. Their operation in biological environment complementing natural biological processes was demonstrated [22]. Multi-step biochemical cascades mimicking electronic circuitries have demonstrated the ability to perform simple arithmetic operations [23–25], play games [26] and make decisions in multi-choice situations [27]. Novel functionalities, supplementary to electronics, achievable in biomolecular systems are the most challenging goals of this research [28, 29]. These systems are still far away from the natural information processing in cells, but are already much more complex than pure synthetic molecular systems [30]. Recent research in unconventional computing [1], particularly using molecular [2–5, 7–9, 31] and biomolecular [10, 11, 14, 15, 19, 32] systems has resulted in artificial (bio)chemical systems mimicking Boolean logic operations, including AND, OR, XOR, NAND, NOR and other logic gates. Reversible [33–36], reconfigurable [37, 38] and resettable [39–41] logic gates for processing of chemical signals have been designed using sophisticated synthetic molecules or complex biomolecular assemblies.

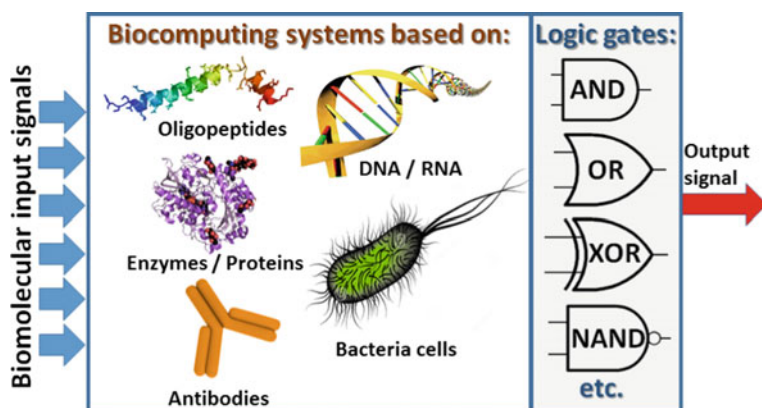


**Fig. 2.1** Biocomputing systems based on various biomolecular/biological species can process multiple chemical input signals and generate an output signal according to different logic implemented in the systems (Adapted from Ref. [30] with permission)

Molecular [33–36, 42, 43] and biomolecular [44–47] systems mimicking operation of reversible logic gates (e.g., Toffoli [44], Fredkin [44–46] and Feynman [34, 35, 47] gates) are of particular interest, since they provide unique output patterns for each combination of input signals. It should be noted that the term “reversibility” in the definition of logic operations has the meaning different from commonly used in chemistry. In information processing the “logic reversibility” means the possibility to recover initial information from the processed information. This is not possible for most of trivial Boolean gates such as AND, OR, etc. Indeed, the logic output **0** can be generated by AND gate for different input combinations: **0, 0**; **0, 1** and **1, 0**, thus the original pattern of the input signals cannot be recovered when the output signal **0** is generated. Special property of logic reversibility can be achieved when the number of channels for the output and input signals is the same, for example, 2-input/2-output, 3-input/3-output. In such case each combination of the input signals can produce a unique pattern of the output signals that allows recovering the initial inputs. Depending on the signal processing function, which is unique to the specific reversible logic gate, the output signals will change differently when various combinations of the inputs are applied. Using this change, the unknown input signals can always be recovered from the measured output signals if the logic function is known. This inherent property of reversible logic gates is important, particularly for biosensing applications of logic gates [48, 49] when all the information in regards to the inputs is needed. For example, medical analysis of biomarkers signaling on injuries [49] can be performed using AND logic gates combining together two biomarkers of low specificity. The decision about the medical conditions, e.g., specific kind of injury, would be based on the simultaneous presence of two biomarkers appearing at concentrations above specific thresholds. While this is enough for the medical conclusion about the presence of the injury conditions, the negative result (logic output **0**) has no clear meaning because it can originate from various combinations of biomarkers, when one or both of them appear below the thresholds. Knowing exactly the original combination of the biomarkers would be the great advantage for biomedical applications. This could be achievable with the use of reversible logic gates.

While justifying the importance of reversible logic gates another inherent physical property that is frequently emphasized is the ability to save energy. During irreversible logic computations, each bit of information lost generates  $kT \ln 2$  joules of heat energy based on thermodynamic consideration [50]. This release of heat results in serious problems for computer engineering, particularly with densely packed nanosized elements. Theoretically [51, 52] and experimentally [53], in some electronic realizations, reversible information processing should not be accompanied by an entropy increase [54], thus classifying it as an energy saving process. This is considered to be a very important feature of reversible information processing, and will be needed in future electronic computers to allow fast computing in nano-scale elements without generation of heat. However, this is not applicable to chemical systems where energy dissipation is inevitable. Therefore, the molecular/biomolecular realizations of reversible logic gates keep only *logic* reversibility, while the energy savings are illusory goals. This rather trivial and obvious conclusion should not be overlooked

when conceiving and/or implementing reversible logic gates in (bio)molecular systems [44].

In order to be useful in a practical sense, reversible logic gates should be integrated in complex information processing networks, which include multi-step Boolean and non-Boolean operations. Unfortunately, some of the experimentally realized systems were all-photonic [43], where the input/output signals were optical signals. This does not allow for easy integration with molecular networks, thus resulting in standalone operations of the gates. Other reversible logic gates used chemical input signals (e.g., metal ions) [33–36], which cannot be easily produced by preceding chemical reactions. This makes integration of the designed reversible gates in complex logic networks very difficult. Although these systems illustrate novel functions, it is certainly not enough for any practical application. Only a few recent experimental examples have demonstrated reversible logic operations with input/output signals that are represented by biomolecules using DNA [44, 46] and enzyme [47] reactions, thus allowing for the extension of information processing and integration of reversible logic gates into complex biomolecular networks that can be designed to mimic biological systems.

Recently designed logic networks based on enzyme-biocatalyzed multi-step reactions [19, 55, 56] are the easiest for the practical realization of systems where logic operations are particularly useful in biomedical sensing [48, 49] as well as diagnostic applications [57, 58]. Despite the fact that complex multi-input/multi-step information processing systems have been successfully realized with enzymatic cascades [19], the requirement of several independently read output signals for realization of reversible logic gates is not a simple task. Cross-talking between enzymatic pathways and chemically produced output signals limit the complexity of the enzyme-based logic systems when they are realized in a homogeneous system. In order to assemble more complex systems for realization of reversible logic gates, “clocking” (temporal control) and spatial separation (compartmentalization) [36] of various steps (e.g., in flow devices) are needed [59, 60]. The present chapter reports on the first experimental realization of reversible logic gates [61] (Feynman gate (Controlled NOT) with 2-input/2-output channels, Double Feynman gate, Toffoli gate and Peres gate with 3-input/3-output channels) using enzyme biocatalytic reactions which are performed in modular flow systems, where the chemical inputs and outputs may be potentially extended to include additional information processing steps, thus allowing for further increase of system complexity. The studied systems were composed of simple single-enzyme-functionalized cells connected in specific networks with a modular design and are presented in the chapter in the order of increasing of their complexity.

## 2.2 Results and Discussion

Figure 2.2a shows a single flow cell which was used for assembling flow devices mimicking the operation of reversible logic gates. The cells were each modified with one immobilized enzyme, before they were assembled in circuitries to organize

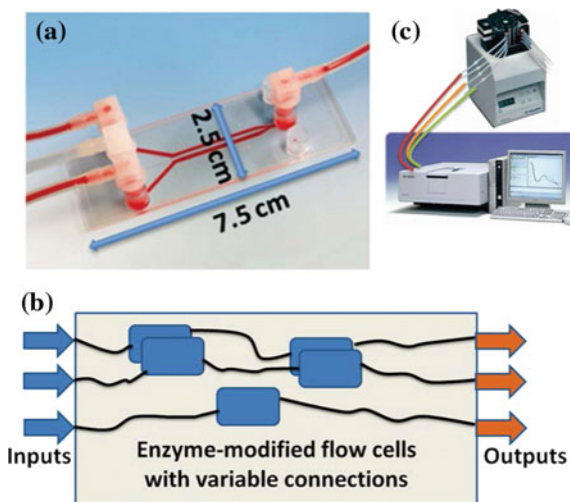


**Fig. 2.2** **a** A single flow cell used as a component of the system. **b** Schematic of the system with many interconnected enzyme-modified cells assembled in a circuitry with variable connections to mimic different logic gates (the scheme does not correspond to any specific logic network; for specific circuitries see Figs. 2.3, 2.6 and 2.9). **c** Spectrophotometer connected to the flow system with help of a multi-channel peristaltic pump (Adapted from Ref. [66] with permission)

biocatalytic cascades composed of several interconnected biocatalytic cells, Fig. 2.2b. For realizing different logic gates, Feynman gate (Controlled NOT; CNOT) Double Feynman gate (DFG), Toffoli gate and Peres gate, the physical layout of the flow circuitries varied depending on the needs of the logic operations. The flow systems that were composed of several interconnected cells had three input and three output channels. The input channels were connected to test-tubes filled with stock solutions of the input signal chemicals, while the output channels were connected to the flow-cuvette in the spectrophotometer for optical reading of the output signals, Fig. 2.2c. The flow of reacting species moving from one enzyme-modified cell to another and finally to the spectrophotometer was maintained with a peristaltic pump.

The following biocatalytic enzymes and substrate-inputs were used to perform reversible logic operations described in the following sections:

*Enzymes immobilized in flow cells:* alkaline phosphatase (AP; E.C. 3.1.3.1) from bovine intestinal mucosa, glucose-6-phosphate dehydrogenase (G6PDH; E.C. 1.1.1.49) from *Leuconostoc mesenteroides*, glucose dehydrogenase (GDH; E.C. 1.1.1.47) from *Pseudomonas sp.*, lactate dehydrogenase (LDH; E.C. 1.1.1.27) from porcine heart, glucose oxidase (GOx; E.C. 1.1.3.4) from *Aspergillus niger*, peroxidase from horseradish (HRP; E.C. 1.11.1.7) and diaphorase from *Clostridium kluyveri* (Diaph; E.C. 1.8.1.4). *Substrates/cofactors used as input signals:* p-nitrophenyl phosphate (PNPP), glucose (Glc), glucose-6-phosphate (G6P), pyruvate (Pyr),  $\beta$ -nicotinamide adenine dinucleotide hydrate ( $\text{NAD}^+$ ),  $\beta$ -nicotinamide adenine dinucleotide reduced dipotassium salt (NADH) and hydrogen peroxide ( $\text{H}_2\text{O}_2$ ).

### 2.2.1 Feynman Gate—Controlled NOT (CNOT) Gate

Here we illustrate the realized Feynman gate (Controlled NOT (CNOT) gate) [47], which is the only non-trivial reversible gate with two input and two output signals [62]. The first experimental realization of a CNOT gate was accomplished in 1995 [63]. Since its realization the CNOT gate has been implemented in many physical systems. This implementation demonstrates great importance for future quantum computing [64], however, it was never researched in chemical, particularly in biochemical, systems aiming at its integration with biomolecular logic networks. Figure 2.3a shows the truth table of the CNOT gate. The CNOT gate flips the second Input  $B$  (the target input) and directs it to the second Output  $Q$  (the target output) if and only if the first Input  $A$  (the control input) is **1**, while the first Input  $A$  is always copied to Output  $P$  (the control output). In other words, Output  $P$  represents an Identity gate for Input  $A$ , while Output  $Q$  is processing Inputs  $A$  and  $B$  according to a XOR logic operation. The logic scheme illustrating CNOT operation is shown in Fig. 2.3b–d, where Input  $A$  is directed to an Identity gate and a XOR gate is activated by both Inputs  $A$  and  $B$ . In our experimental realization we defined Input  $A$  as a Tris-buffer solution (0.1 M, pH 7.1) containing p-nitrophenyl phosphate (PNPP) and pyruvate (Pyr) with concentrations 10 and 1 mM, respectively, to represent logic **1** value. Logic **0** value for Input  $A$  was defined as the absence of PNPP and Pyr in the solution. Input  $B$  was defined as a Tris-buffer solution (0.1 M, pH 7.1) containing glucose-6-phosphate (G6P), 6mM, for logic **1** value. The absence of G6P was used to encode logic **0** for Input  $B$ . Note that the concentrations of the reacting species were optimized experimentally as will be described later. PNPP representing one of the reacting species in Input  $A$

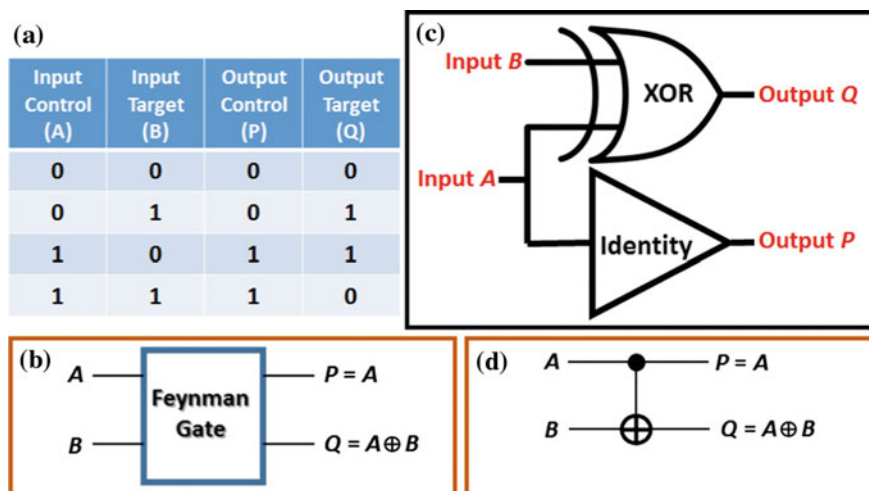


**Fig. 2.3** The truth table (a), block diagram (b), logic circuitry (c) and equivalent electronic circuitry (d) for Feynman (CNOT) gate

was converted to p-nitrophenol (PNP) in the reaction biocatalyzed by alkaline phosphatase (AP) resulting in the optical absorbance increase ( $\lambda_{\max} = 420 \text{ nm}$ ), Fig. 2.4. This biocatalytic reaction represented the Identity gate, Fig. 2.3c, and the produced absolute values of absorbance changes were used as Output *P*, which was defined as logic **1** or **0** when  $|\Delta\text{Abs}| > 0.1$  or  $|\Delta\text{Abs}| < 0.1$ , respectively. Input *A* was also directed to the biochemical system performing a XOR logic operation, Fig. 2.3c.

We designed a XOR gate with two oppositely directed biocatalytic redox reactions [65] activated by pyruvate (Pyr; second reacting species in Input *A*) and glucose-6-phosphate (G6P; Input *B*), Fig. 2.4. Input *B* was defined as logic **0** and **1** for absence of G6P and its presence with the concentration of 6 mM, respectively. The reaction media (all input solutions) also included NADH (0.4 mM) and  $\text{NAD}^+$  (10 mM) cofactors as a part of the gate “machinery”. NADH was oxidized by Pyr in the reaction biocatalyzed by lactate dehydrogenase (LDH) producing  $\text{NAD}^+$  and decreasing the NADH absorbance at  $\lambda_{\max} = 340 \text{ nm}$ .  $\text{NAD}^+$  was reduced by G6P in the reaction biocatalyzed by glucose-6-phosphate dehydrogenase (G6PDH) producing NADH and increasing its absorbance. Output *Q* produced by the XOR gate, Fig. 2.3c, was measured as absolute values of the absorbance changes at  $\lambda_{\max} = 340 \text{ nm}$  and defined as logic **1** and **0** for  $|\Delta\text{Abs}| > 0.2$  or  $|\Delta\text{Abs}| < 0.2$ .

The Identity and XOR gates operating in parallel were realized in a flow system schematically outlined in Fig. 2.4. The biocatalytic reactions proceeding in the flow cells are shown schematically in each box representing a single cell, Fig. 2.4. Figure 2.5 shows a photo of the experimental setup for realization of the Feynman gate (CNOT) gate. The solutions containing biochemicals representing Inputs *A* and *B* with the variable binary logic values **0** and **1**, as well as the constant composition of the “machinery” represented by mixed NADH/ $\text{NAD}^+$  were pumped through flow devices containing immobilized enzymes biocatalyzing chemical transformations mimicking logic operations. The flow design of the biochemical device allowed “clocking” (temporal control) and spatial separation of the reaction steps. While the Identity gate realized in a single flow unit performed a simple biocatalytic transformation of PNPP to PNP yielding an optically readable signal, the XOR gate was composed of two flow-through units: one modified with G6PDH that was reducing  $\text{NAD}^+$  when G6P was available; another modified with LDH was oxidizing NADH

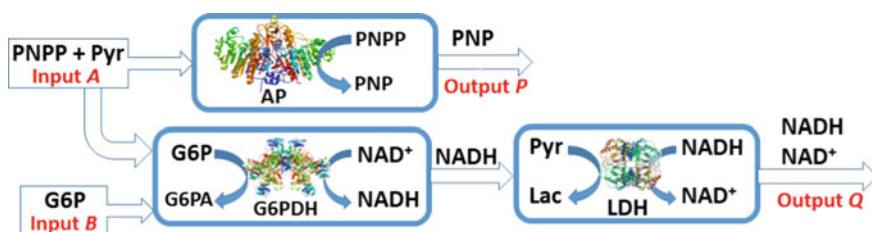
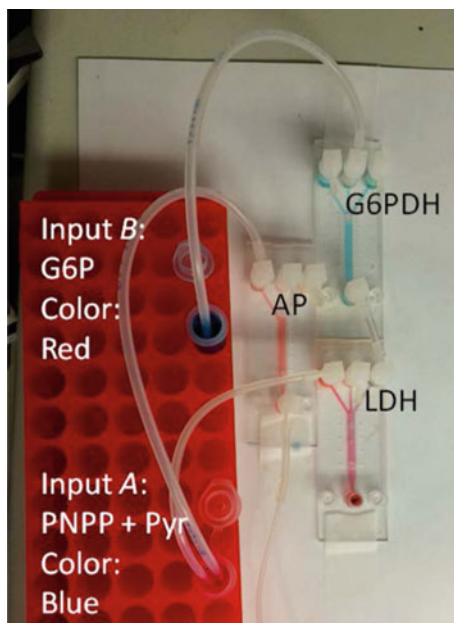


**Fig. 2.4** The biocatalytic cascade mimicking the CNOT gate operation (G6PA—6-phosphogluconic acid; Lac—lactate; all other abbreviations and reactions are explained in the text)



**Fig. 2.5** The experimental setup for realization of the Feynman (CNOT) gate. Please note different colored dyes used to illustrate experimental realization and mixing where applicable (Adapted from Ref. [47] with permission)



in the presence of Pyr, Fig. 2.4. Therefore, the optical absorbance corresponding to the NADH concentration was decreasing in the presence of Pyr and absence of G6P (input combination **1, 0**) and increasing in the absence of Pyr and presence of G6P (input combination **0, 1**). Since the NADH concentration and the corresponding absorbance were changed in different directions (decreasing and increasing), the Output  $Q$  value **1** was defined as the absolute value of the absorbance change. The flow cells modified with G6PDH and LDH were optimized (balanced) in such a way that simultaneous presence of Pyr and G6P (input combination **1, 1**) resulted in no changes in the concentration of NADH, meaning logic value **0** for Output  $Q$ . Balancing of the biocatalytic reaction rates was achieved by optimization of input concentrations for Pyr and G6P for the specific activity of the enzymes immobilized in the flow units. Obviously, the absence of Pyr and G6P (input combination **0, 0**) did not result in any reaction and preserved the NADH absorbance unchanged resulting in logic **0** for Output  $Q$ . These biocatalytic processes performed in the flow system allowed operation of the XOR part of the CNOT gate. It should be noted that the absorbance measurements for the solutions reacted in the flow device were performed versus the “machinery” solution containing NADH/NAD<sup>+</sup> applied to the reference channel of the spectrophotometer, thus reflecting absorbance difference in the reacting solutions rather than their full absorbance.

Figure 2.6 shows the experimental data obtained upon application of the input signals in different logic combinations. Figure 2.6A shows the absorbance changes observed in the Output  $P$  (from the Identity gate). In the absence of PNPP only minor absorbance changes were observed, meaning an Output  $P$  logic **0** value. Each



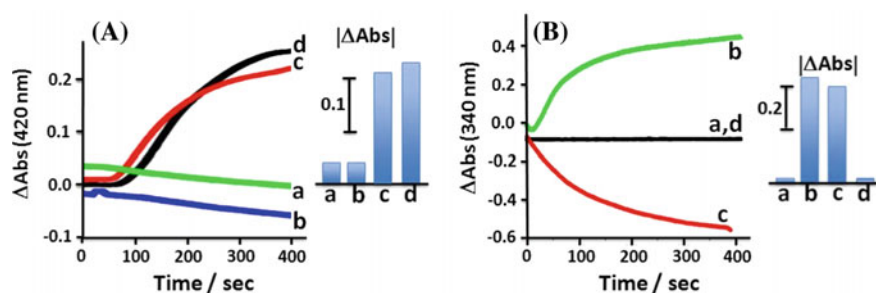


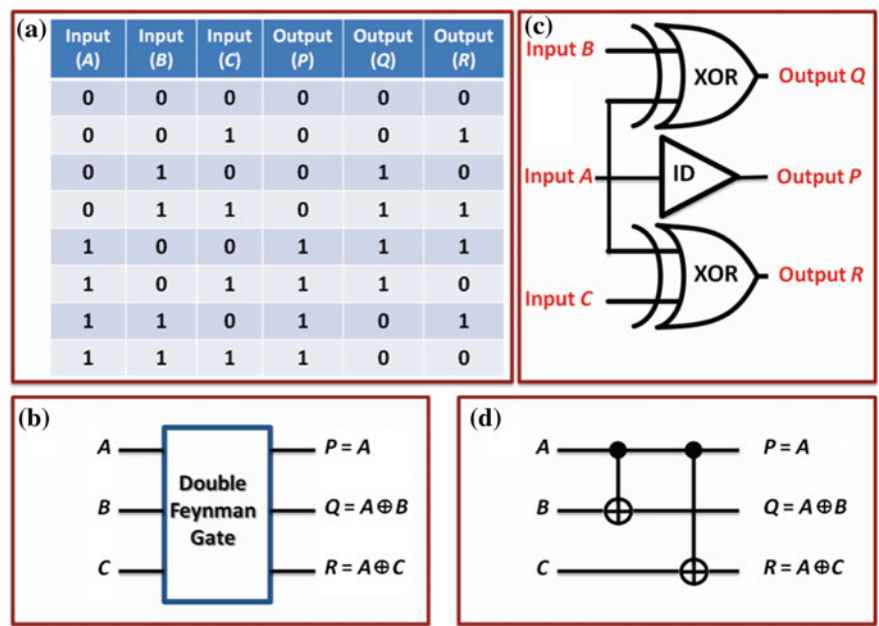
**Fig. 2.6** A, B Optical responses of the Identity and XOR parts of the CNOT gate, respectively, upon application of input combinations: *a* 0, 0; *b* 0, 1; *c* 1, 0 and *d* 1, 1. *Insets* show the optical outputs obtained after 400 s of the flow system operation (Adapted from Ref. [47] with permission)

time application of PNPP (regardless presence or absence of any other species) resulted in the absorbance increase at  $\lambda_{\text{max}} = 420\text{ nm}$  reflecting the formation of PNP and resulting in the output logic **1**; thus, Input *A* was directly copied to Output *P*. Figure 2.6B shows the XOR gate performance where only unbalanced input signals **0, 1** and **1, 0** resulted in the absorbance changes (output **1**), while the absence of the reacting Pyr and G6P (inputs **0, 0**) or their balanced application (inputs **1, 1**) resulted in no absorbance changes (output **0**).

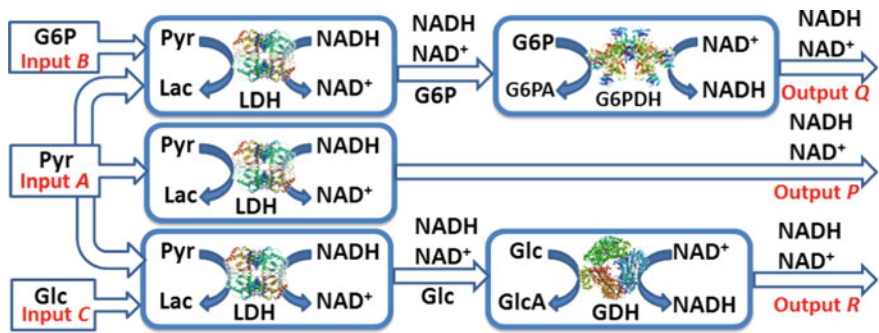
### 2.2.2 Double Feynman Gate (DFG) Operation

Figure 2.7a shows the truth table of DFG. DFG operates with three input and three output signals, where Input *A* is copied to Output *P*, while two other output signals *Q* and *R* are the results of two XOR logic functions performed on Inputs *A, B* and *A, C*, respectively, Fig. 2.7b. In other words, DFG can be represented as the Identity (ID) gate and two XOR gates operating in parallel, Fig. 2.7c, d. Therefore, when realized in a biochemical system [66], the DFG is a very convenient example of a parallel computing system. This convenience is illustrated by the simplistic design of the gate as a flow-through device with parallel channels.

The ID and two XOR gates operating in parallel were realized in a flow system outlined in Fig. 2.8. The solutions containing biochemicals, pyruvate (Pyr), glucose-6-phosphate (G6P) and glucose (Glc) representing Inputs *A, B* and *C*, respectively, with the variable binary logic values **0** and **1**, as well as the constant composition of the “machinery” represented by mixed NADH/NAD<sup>+</sup> were pumped through the flow devices containing immobilized enzymes biocatalyzing chemical transformations mimicking logic operations. The flow design of the biochemical device allowed “clocking” (temporal control) and spatial separation of the reaction steps. While the ID gate realized in a single flow unit performed a simple biocatalytic transformation (NADH oxidation) yielding an optically readable signal, the XOR gates were



**Fig. 2.7** The truth table (a), block diagram (b), logic circuitry (c) and equivalent electronic circuitry (d) for Double Feynman gate (DFG) (Adapted from Ref. [66] with permission)



**Fig. 2.8** Experimental realization of the biocatalytic Double Feynman gate (DFG) in the flow device (GlcA—gluconic acid, Lac—lactate, G6PA—6-phosphogluconic acid; all other abbreviations and processes are explained in the text). (Adapted from Ref. [66] with permission)

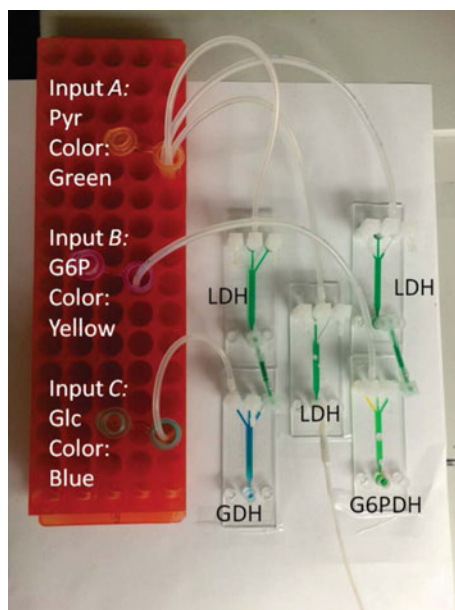
composed of two flow-through units connected in serial: one modified with the enzyme oxidizing NADH to yield NAD<sup>+</sup> and another with the enzyme reducing NAD<sup>+</sup> resulting in the formation of NADH, thus decreasing and increasing optical absorbance corresponding to NADH concentration. The input signals were applied to the 3-channel flow system, where the biocatalytic reactions were performed in

parallel, Fig. 2.8. The biocatalytic reactions proceeding in the flow cells are shown schematically in each box representing a single cell, Fig. 2.8.

Input *A* represented by Pyr was applied to the flow cell functionalized with LDH, Fig. 2.8. Pyr, if it is present in Input *A* (logic **1** value), resulted in the oxidation of NADH in the reaction biocatalyzed by LDH, thus resulting in the optical absorbance decrease ( $\lambda_{\text{max}} = 340\text{ nm}$ ). In the absence of Pyr (logic **0** value) the NADH oxidation was not possible and the absorbance was not changed. This biocatalytic reaction represented the ID gate, Fig. 2.7c, and the produced absolute values of absorbance changes were used as Output *P*, which was defined as logic **1** or **0** when  $|\Delta\text{Abs}| > 0.2$  or  $|\Delta\text{Abs}| < 0.2$ , respectively. Input *A* (Pyr) was also directed to biochemical systems performing XOR logic operations, Fig. 2.7c. The first XOR channel was fed with Inputs *A* and *B* (Pyr and G6P, respectively). This channel was composed of two flow cells functionalized with LDH and G6PDH operating in sequence, Fig. 2.8. The XOR gate was designed to operate with two oppositely directed biocatalytic redox reactions [65] activated by Pyr and G6P. In the presence of Pyr, NADH was oxidized in the reaction biocatalyzed by LDH in the first flow cell, thus decreasing its absorbance at 340 nm. On the other hand, in the presence of G6P,  $\text{NAD}^+$  was reduced in the reaction biocatalyzed by G6PDH in the second flow cell, thus increasing absorbance at 340 nm corresponding to the formation of NADH. Output *Q* in this channel was measured as absolute values of the absorbance changes at  $\lambda_{\text{max}} = 340\text{ nm}$  and defined as logic **1** and **0** for  $|\Delta\text{Abs}| > 0.2$  or  $|\Delta\text{Abs}| < 0.2$ , respectively. The second XOR channel was activated with Inputs *A* and *C* (Pyr and Glc, respectively). This channel was composed of two flow cells functionalized with LDH and GDH operating in sequence, Fig. 2.8. This XOR gate was also designed to operate with two opposite biocatalytic reactions. In the presence of Pyr, NADH was oxidized in the reaction biocatalyzed by LDH in the first flow cell, thus decreasing its absorbance at 340 nm. In the presence of Glc,  $\text{NAD}^+$  was reduced in the reaction biocatalyzed by GDH in the second flow cell, thus increasing absorbance at 340 nm corresponding to the formation of NADH. Output *R* in this channel was measured as absolute values of the absorbance changes at  $\lambda_{\text{max}} = 340\text{ nm}$  and defined as logic **1** and **0** for  $|\Delta\text{Abs}| > 0.2$  or  $|\Delta\text{Abs}| < 0.2$ , respectively. Figure 2.9 shows the experimental setup for realization of the DFG.

The flow cells modified with enzymes oxidizing NADH and reducing  $\text{NAD}^+$  were optimized (balanced) in such a way that simultaneous presence of the oxidizing input (Pyr) and reducing input (G6P or Glc) (input combination **1, 1**) resulted in negligible overall changes in the concentration of NADH, meaning logic value **0** for Outputs *Q* and *R*. Balancing of the biocatalytic reaction rates was achieved by optimization of input concentrations for Pyr and G6P in one channel and Pyr and Glc in another channel for the specific activity of the enzymes immobilized in the flow units. Obviously, the absence of Pyr and G6P or Glc (input combinations **0, 0**) did not result in any reaction and preserved the NADH absorbance unchanged resulting in logic **0** for Outputs *Q* and *R*. The unbalanced input signals (**0, 1** or **1, 0**) applied to the XOR channels resulted in the NADH absorbance changes considered as the output signal **1**. These biocatalytic processes performed in the flow system allowed operation of the XOR parts of DFG. It should be noted that the absorbance

**Fig. 2.9** Experimental realization of DFG (photo of the flow cell circuitry). Different colored dyes are used in this image to illustrate the experimental realization including the mixing of channels where it is applicable (Adapted from Ref. [66] with permission)

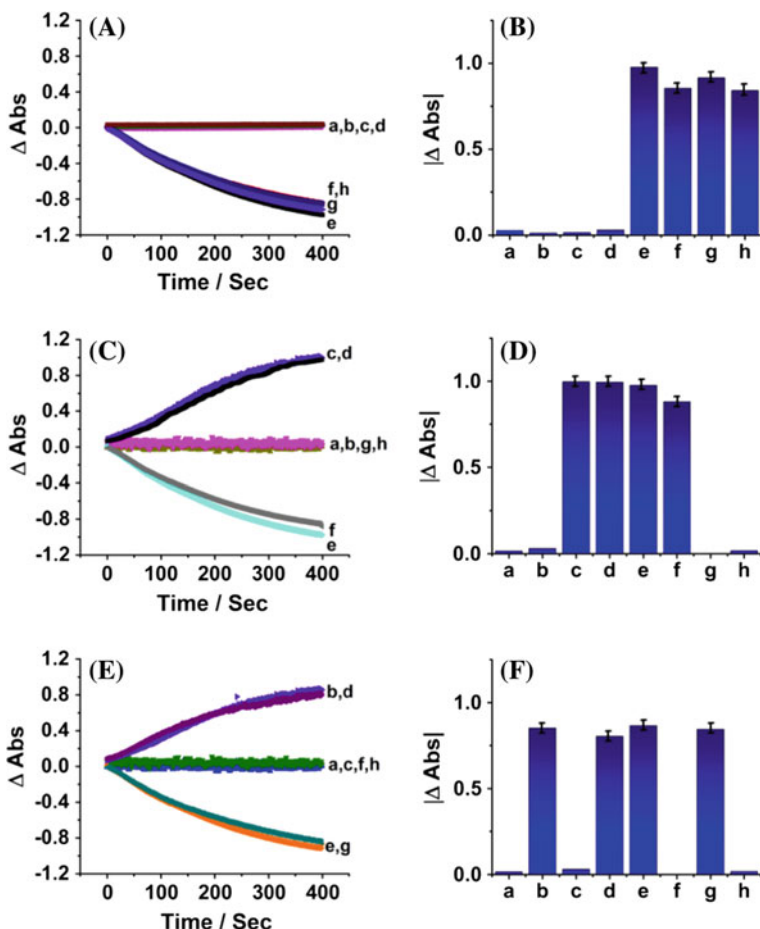


measurements for the solutions reacted in the flow device were performed versus the “machinery” solution containing a constant amount of NADH/NAD<sup>+</sup> applied to the reference channel of the spectrophotometer, thus reflecting the absorbance difference in the reacting solutions rather than their full absorbance.

Figure 2.10 shows the experimental data obtained upon application of the input signals in 8 different logic combinations. Figure 2.10A, B shows the absorbance changes observed in Output *P* (from the ID gate). In the absence of Pyr no absorbance changes were observed, meaning a logic **0** value for Output *P*. Each application of Pyr (regardless presence or absence of any other species) resulted in the decrease of absorbance at  $\lambda_{\text{max}} = 340 \text{ nm}$ , thus reflecting the oxidation of NADH and resulting in the output logic **1**. Figure 2.10C, D and E, F show the XOR gate performance where only unbalanced *A*, *B* and *A*, *C* input signals (**0**, **1** and **1**, **0**) resulted in the change of absorbance (output **1**), while the absence of the reacting species (inputs **0**, **0**) or their balanced application (inputs **1**, **1**) resulted in no change of absorbance (output **0**). Overall, the obtained experimental data show the output signal pattern, Fig. 2.10, corresponding to the truth table, Fig. 2.7a, characteristic of DFG.

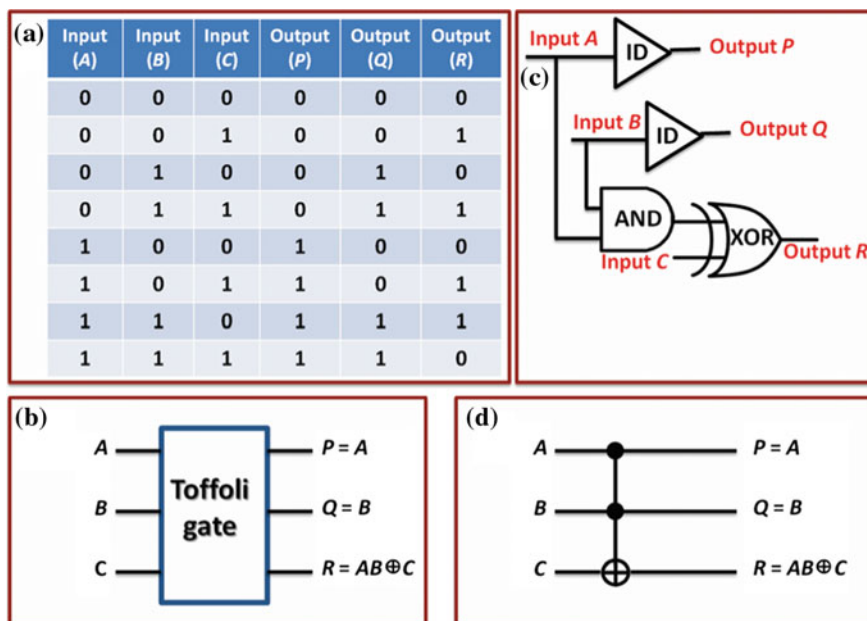
### 2.2.3 Toffoli Gate Operation

Figure 2.11a shows the truth table of Toffoli gate. Toffoli gate operates with three input and three output signals, where Inputs *A* and *B* are directly copied to Outputs



**Fig. 2.10** Optical responses of the Double Feynman gate (DFG) system to various combinations of the input signals: *a* 0, 0, 0; *b* 0, 0, 1; *c* 0, 1, 0; *d* 0, 1, 1; *e* 1, 0, 0; *f* 1, 0, 1; *g* 1, 1, 0; *h* 1, 1, 1. (Note that the logic values are shown for the input signals in the following order: *A*, *B*, *C*.) **A**, **B** panels show *P* output corresponding to the Identity operation copying *A* input signal. **C**, **D** panels show *Q* output corresponding to the XOR operation on *A* and *B* inputs. **E**, **F** panels show *R* output corresponding to the XOR operation on *A* and *C* inputs. **A**, **C** and **E** plots show kinetics of the signal generation. **B**, **D** and **F** bar charts show the signals obtained after 400s of the flow system operation. All output signals were read at  $\lambda_{\text{max}}$  340nm. The data shown in the bar-charts are average of three independent experiments (Adapted from Ref. [66] with permission)

*P* and *Q*, thus representing two ID gates operating in parallel. In addition to their role in the ID gates, Inputs *A* and *B* are directed to an AND gate to generate an intermediate output which is then directed to a XOR gate together with Input *C* to yield Output *R*, Fig. 2.11b–d. In other words, Toffoli gate can be represented as two ID gates operating in parallel with the AND-XOR concatenated gates, Fig. 2.11c.



**Fig. 2.11** The truth table (a), block diagram (b), logic circuitry (c) and equivalent electronic circuitry (d) for Toffoli gate (Adapted from Ref. [66] with permission)

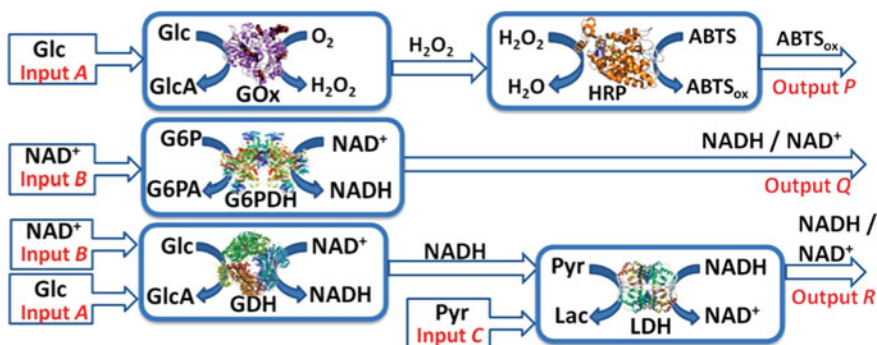
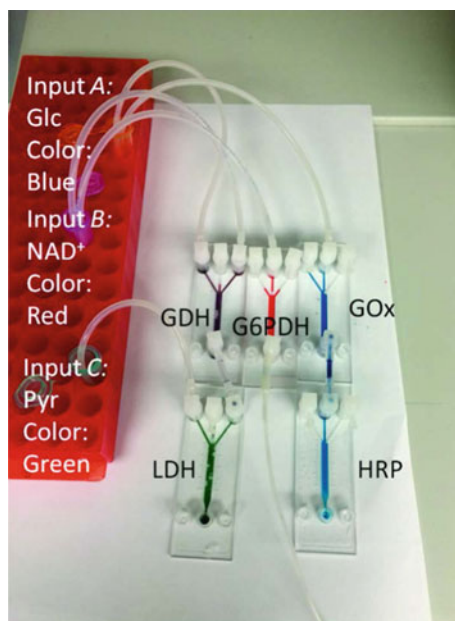


**Fig. 2.12** Experimental realization of the biocatalytic Toffoli gate in the flow device (GlcA—gluconic acid, Lac—lactate, G6PA—6-phosphogluconic acid; all other abbreviations and processes are explained in the text) (Adapted from Ref. [66] with permission)

Two ID gates and the AND-XOR concatenated gates operating in parallel were realized [66] in a flow system outlined in Fig. 2.12. Figure 2.13 shows a photo of the experimental setup for realization of the Toffoli gate. The solutions containing biochemicals, Glc,  $\text{NAD}^+$  and Pyr, representing Inputs A, B and C, respectively, with the variable binary logic values **0** and **1**, as well as the constant composition of the “machinery” that is represented by a mixture of  $\text{NADH}/\text{G6P}/\text{ABTS}$  (note that



**Fig. 2.13** Experimental realization of Toffoli gate (photo of the flow cell circuitry). Different colored dyes are used in this image to illustrate the experimental realization including the mixing of channels where it is applicable (Adapted from Ref. [66] with permission)



$O_2$  was always present in the solution in equilibrium with air) were pumped through flow cells containing immobilized enzymes biocatalyzing chemical transformations mimicking logic operations. The first ID gate activated by Input A was composed of two flow cells operating in sequence: the first cell modified with GOx produced  $H_2O_2$  in the presence of glucose (Glc) (if Input A was applied at logic value **1**). Then for convenient optical detection, the produced  $H_2O_2$  was reacted with ABTS in the second flow cell modified with HRP to yield colored oxidized ABTS ( $ABTS_{ox}$ ) which represented Output P. Obviously, in the absence of glucose (logic value **0** for Input A)  $H_2O_2$  was not produced and ABTS was not oxidized, thus preserving the optical absorbance in this channel without changes. Output P in this channel was measured as the absorbance changes at  $\lambda_{max} = 415$  nm characteristic of  $ABTS_{ox}$  and defined as logic **1** and **0** for  $\Delta Abs > 0.2$  or  $\Delta Abs < 0.2$ , respectively. The second ID gate activated with Input B was represented by a single flow cell modified with G6PDH. In the presence of  $NAD^+$  (logic value **1** for Input B) this cell produced NADH (note that the reducing species G6P were always present in the “machinery” solution) which was considered as Output Q. In the absence of  $NAD^+$  (logic value **0** for Input B) NADH was not produced, thus keeping the initial absorbance without changes. It should be noted that NADH was also present in the “machinery” solution, thus the NADH produced in the flow cells was added to the background amount of NADH. Output Q in this channel was measured as absolute values of the absorbance changes at  $\lambda_{max} = 340$  nm characteristic of NADH and defined as logic **1** and **0** for  $|\Delta Abs| > 0.2$  or  $|\Delta Abs| < 0.2$ , respectively. Overall, Inputs A and B were directly copied to Outputs P and Q.



The AND gate was activated with a combination of Inputs *A* and *B* (Glc and  $\text{NAD}^+$ , respectively). In the presence of both reacting species (inputs **1, 1**), GDH catalytically reduced  $\text{NAD}^+$  to NADH, which was moving with the flow to the next cell modified with LDH. If either or both reacting species were absent (inputs **0, 1**; **1, 0**; **0, 0**) NADH was not produced, thus demonstrating the AND logic features. The cell functionalized with LDH was additionally fed with Input *C* (Pyr). If both reacting species (NADH and Pyr) were present (**1, 1, 1** combination for Inputs *A*, *B*, *C*), the reaction biocatalyzed by LDH resulted in oxidation of NADH, thus bringing its concentration down to the original level and keeping the optical absorbance with no changes (Output *R* **0**). It should be noted that the Pyr concentration was carefully optimized to keep the balance and to compensate the NADH production in the first reacting cell. The same result was achieved if no reactions were activated in both connected flow cells (**0, 0, 0** combination for Inputs *A*, *B*, *C*). When NADH was produced in the first cell but Pyr was not present (**1, 1, 0** combination for Inputs *A*, *B*, *C*) Output *R* demonstrated increasing absorbance corresponding to the produced NADH (Output *R* **1**). When NADH was not produced in the first cell, but Pyr was present (**0, 0, 1**; **0, 1, 1**; **1, 0, 1** combinations for Inputs *A*, *B*, *C*) the reaction in the second cell resulted in the consumption of NADH present in the background solution, thus resulting in the absorbance decrease. Output *R* in this channel was measured as absolute values of the absorbance changes at  $\lambda_{\text{max}} = 340 \text{ nm}$  characteristic of NADH and defined as logic **1** and **0** for  $|\Delta\text{Abs}| > 0.2$  or  $|\Delta\text{Abs}| < 0.2$ , respectively.

Figure 2.14 shows the experimental data obtained upon application of the input signals in 8 different logic combinations. Figure 2.14A, B shows the absorbance changes observed in Output *P* (from the first ID gate). In the absence of Glc no absorbance changes were observed, meaning logic **0** value for Output *P*. Each application of Glc (regardless presence or absence of any other species) resulted in the increase of absorbance at  $\lambda_{\text{max}} = 415 \text{ nm}$ , reflecting the oxidation of ABTS and resulting in the output logic **1**. Figure 2.14C, D shows the absorbance changes observed in Output *Q* (from the second ID gate). In the absence of  $\text{NAD}^+$  no absorbance changes were observed, meaning logic **0** value for Output *Q*. When  $\text{NAD}^+$  was applied (regardless presence or absence of any other species) the absorbance at  $\lambda_{\text{max}} = 340 \text{ nm}$  was increased corresponding to the production of NADH and resulting in the output logic **1**. Figure 2.14E, F shows the AND-XOR gates performance where only unbalanced *A*, *B* and *C* input signals (**0, 0, 1**; **0, 1, 1**; **1, 0, 1**; **1, 1, 0**) resulted in the change of absorbance (output **1**), while the absence of the reacting species (inputs **0, 0, 0**) or their balanced application (inputs **0, 1, 0**; **1, 0, 0**; **1, 1, 1**) resulted in no change of absorbance (output **0**). Overall, the obtained experimental data show the output signal pattern, Fig. 2.14, corresponding to the truth table, Fig. 2.11a, characteristic of Toffoli gate.

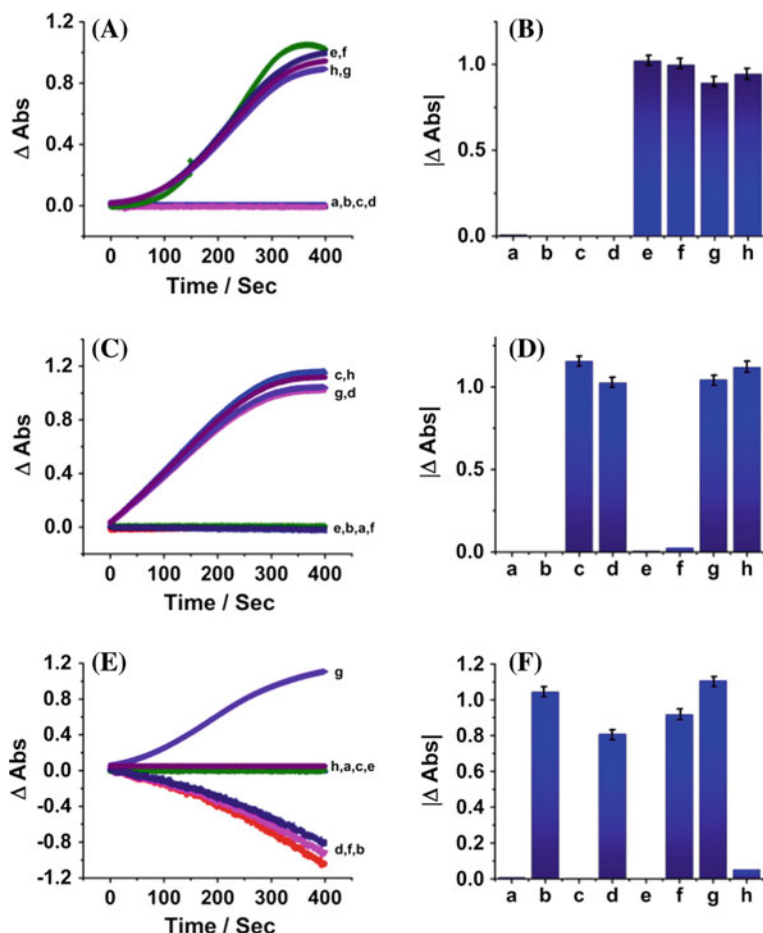


**Fig. 2.14** Optical responses of the Toffoli gate system to various combinations of the input signals: *a* 0, 0, 0; *b* 0, 0, 1; *c* 0, 1, 0; *d* 0, 1, 1; *e* 1, 0, 0; *f* 1, 0, 1; *g* 1, 1, 0; *h* 1, 1, 1. (Note that the logic values are shown for the input signals in the following order: *A*, *B*, *C*.) **A**, **B** panels show *P* output corresponding to the Identity operation copying *A* input signal. **C**, **D** panels show *Q* output corresponding to the Identity operation copying *B* input signal. **E**, **F** panels show *R* output corresponding to the AND operation on *A* and *B* inputs followed by the XOR operation on the output from the AND gate and *C* input. **A**, **C** and **E** plots show kinetics of the signal generation. **B**, **D** and **F** bar charts show the signals obtained after 400 s of the flow system operation. Output *P* was read at  $\lambda_{\text{max}}$  415 nm and Outputs *Q* and *R* were read at  $\lambda_{\text{max}}$  340 nm. The data shown in the bar-charts are average of three independent experiments (Adapted from Ref. [66] with permission)

## 2.2.4 Peres Gate Operation

Figure 2.15a shows the truth table of Peres gate. Peres gate operates with three input and three output signals, where Input *A* is directly copied to Output *P*, while two

other output signals  $Q$  and  $R$  are the results of complex logic operations. Inputs  $A$  and  $B$  are processed through a XOR gate to yield Output  $Q$ . Inputs  $A$  and  $B$  are also processed through an AND gate and the resulting intermediate goes to another XOR gate together with Input  $C$  to generate Output  $R$  at the end of the concatenated logic operations, Fig. 2.15b. In other words, Peres gate can be represented as the ID gate operating in parallel with a XOR gate and an AND-XOR circuit, Fig. 2.15c, d.

The ID, XOR and AND-XOR gates operating in parallel were realized [66] in a flow system outlined in Fig. 2.16. Figure 2.17 shows a photo of the experimental setup for realization of the Peres gate. The solutions containing biochemicals, NADH, Glc and  $\text{H}_2\text{O}_2$ , representing Inputs  $A$ ,  $B$  and  $C$ , respectively, with the variable binary logic values **0** and **1**, as well as the constant composition of the “machinery” represented by mixed  $\text{K}_3[\text{Fe}(\text{CN})_6]$ ,  $\text{K}_4[\text{Fe}(\text{CN})_6]$  and Pyr (note that  $\text{O}_2$  was always present in the solution in equilibrium with air) were pumped through flow cells containing immobilized enzymes biocatalyzing chemical transformations mimicking logic operations. The ID gate activated by Input  $A$  (NADH) was represented with a flow cell functionalized with Diaph which catalyzed NADH oxidation by  $[\text{Fe}(\text{CN})_6]^{3-}$ . This process resulted in the production of reduced  $[\text{Fe}(\text{CN})_6]^{4-}$  and absorbance decrease at  $\lambda_{\text{max}} = 420\text{ nm}$  characteristic of  $[\text{Fe}(\text{CN})_6]^{3-}$  when Input  $A$  was applied at logic **1** value. In the absence of NADH (logic **0**) the reaction did

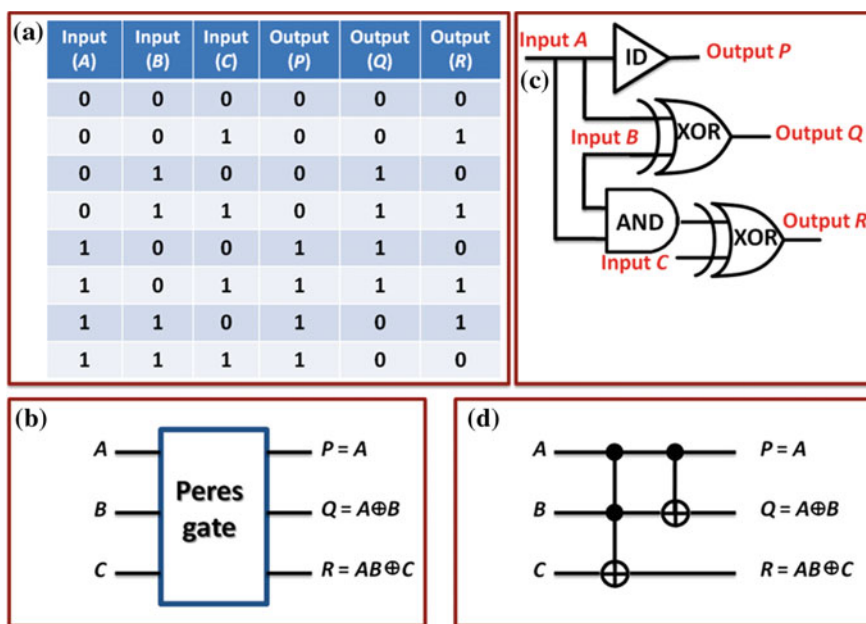


**Fig. 2.15** The truth table (a), block diagram (b), logic circuitry (c) and equivalent electronic circuitry (d) for Peres gate (Adapted from Ref. [66] with permission)

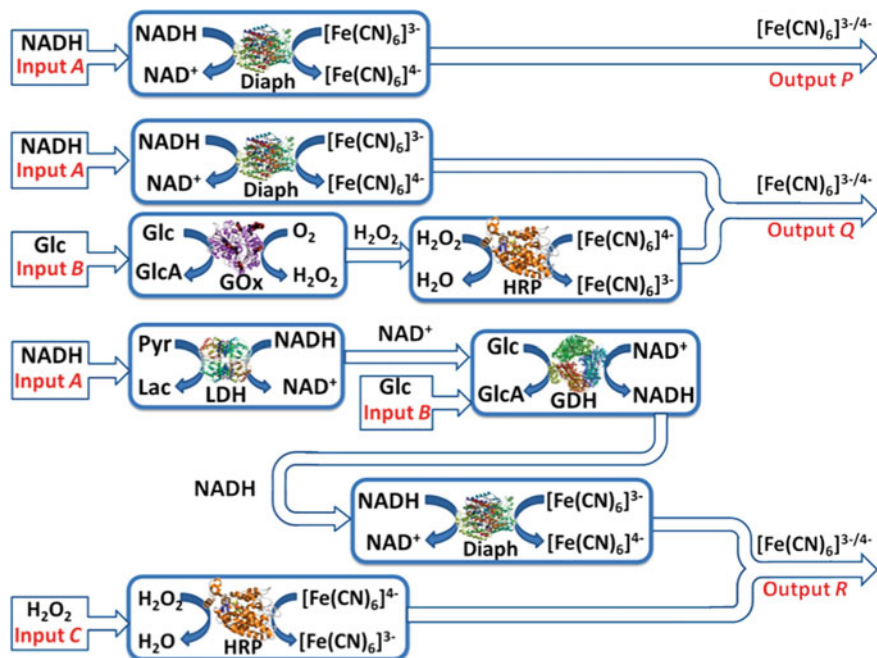
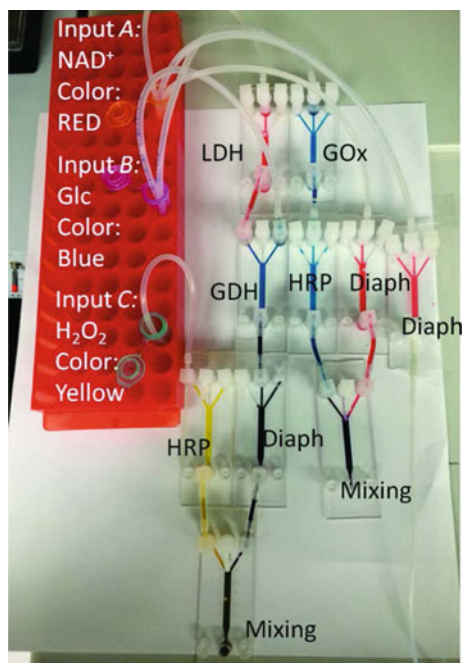


**Fig. 2.16** Experimental realization of the biocatalytic Peres gate in the flow device (GlcA—gluconic acid, Lac—lactate; all other abbreviations and processes are explained in the text) (Adapted from Ref. [66] with permission)

not proceed and the absorbance was not changed regardless of logic values of other inputs.

The XOR gate activated with Inputs *A* and *B* was realized in the following way. Input *A* (NADH) was applied to a flow cell functionalized with Diaph and operating in the way similar to described above. This biocatalytic pathway resulted in the consumption of  $[\text{Fe}(\text{CN})_6]^{3-}$ . Input *B* (Glc) was applied to another flow cell functionalized with GOx. The reaction in this cell resulted in biocatalytic oxidation of glucose and concomitant production of  $\text{H}_2\text{O}_2$  (note that  $\text{O}_2$  was present in the solution). The in situ produced  $\text{H}_2\text{O}_2$  was directed to the next flow cell modified with HRP where  $[\text{Fe}(\text{CN})_6]^{4-}$  was oxidized by  $\text{H}_2\text{O}_2$  to yield  $[\text{Fe}(\text{CN})_6]^{3-}$ . This reaction chain was activated only in the presence of Glc (Input *B* in logic 1 value). The solutions flowing out of the Diaph-modified cell fed with Input *A* and out of the GOx-HRP-modified cells fed with Input *B* were mixed after the biochemical reactions to yield finally Output *Q*. The overall result showed increasing or decreasing absorbance at  $\lambda_{\text{max}} = 420 \text{ nm}$  corresponding to the increasing or decreasing concentration of  $[\text{Fe}(\text{CN})_6]^{3-}$  when Inputs *A* and *B* were applied with the combinations 0, 1 or 1, 0, respectively. When Inputs *A* and *B* were applied at logic values 0, 0 or 1, 1, the overall absorbance was not changed because the final concentration of  $[\text{Fe}(\text{CN})_6]^{3-}$  coming from two parallel channels was not changed due to the absent (0,

**Fig. 2.17** Experimental realization of Peres gate (photo of the flow cell circuitry). Different colored dyes are used in this image to illustrate the experimental realization including the mixing of channels where it is applicable (Adapted from Ref. [66] with permission)



**0** inputs) or balanced (**1, 1** inputs) reactions. Output *Q* in this channel was measured as the absolute values of the absorbance changes at  $\lambda_{\max} = 420$  nm, characteristic of  $[\text{Fe}(\text{CN})_6]^{3-}$  and defined as logic **1** and **0** for  $|\Delta\text{Abs}| > 0.1$  or  $|\Delta\text{Abs}| < 0.1$ , respectively.

The most sophisticated function was realized for Output *R*, Fig. 2.16. First Input *A* (NADH) was processed in the cell modified with LDH where NADH was biocatalytically oxidized with Pyr (note that Pyr was always present in the background solution) to yield  $\text{NAD}^+$  which was then directed to the next cell modified with GDH. In that cell,  $\text{NAD}^+$  was reduced back to NADH in the presence of Input *B* (Glc). The two-step biocatalytic cascade was terminated with the production of NADH if both reaction steps were activated (combination **1, 1** for Inputs *A* and *B*). When NADH input was absent in the first cell (Input *A* **0**) the biocatalytic cascade was not activated at all, regardless of the absence or presence of Glc in the second cell (input combinations **0, 0** and **0, 1** for Inputs *A* and *B*). In the presence of NADH in the first cell modified with LDH and in the absence of Glc in the second cell modified with GDH (combination **1, 0** for Inputs *A* and *B*), the overall result was production of  $\text{NAD}^+$  in the first cell which was not returned back to NADH in the second cell. Thus, the final output in the form of the NADH production after two consecutive cells was only in the presence of both Inputs *A* and *B* in **1, 1** combination, thus demonstrating the features of the AND function. The produced NADH was applied to the next flow cell modified with Diaph where NADH was used to reduce  $[\text{Fe}(\text{CN})_6]^{3-}$  yielding  $[\text{Fe}(\text{CN})_6]^{4-}$ . Another reaction operating in parallel was performed in the cell modified with HRP

where Input *C* ( $\text{H}_2\text{O}_2$ ) oxidized  $[\text{Fe}(\text{CN})_6]^{4-}$  to yield  $[\text{Fe}(\text{CN})_6]^{3-}$ . The solution produced in this cell was mixed with the solution coming out of the cascade of reactions realized in the cells modified with LDH-GDH-Diaph. The solution coming out of HRP-modified cell will increase the  $[\text{Fe}(\text{CN})_6]^{3-}$  concentration if Input *C* is applied at logic value **1** (meaning presence of  $\text{H}_2\text{O}_2$ ). The solution coming out of LDH-GDH-Diaph cells will decrease the  $[\text{Fe}(\text{CN})_6]^{3-}$  concentration if Inputs *A* and *B* are applied at **1, 1** combination. The overall result is the unchanged  $[\text{Fe}(\text{CN})_6]^{3-}$  concentration in case of **0, 0, 0; 0, 1, 0; 1, 0, 0** and **1, 1, 1** combinations for Inputs *A*, *B* and *C* because of the absence of the corresponding reactions or due to their balancing. All other input combinations (**0, 0, 1; 0, 1, 1; 1, 0, 1; 1, 1, 0**) resulted in the  $[\text{Fe}(\text{CN})_6]^{3-}$  concentration change, thus resulting in the corresponding absorbance change. These results correspond to the logic operation of the concatenated AND-XOR gates as needed for the part of Peres gate. Output *R* in this channel was measured as absolute values of the absorbance changes at  $\lambda_{\text{max}} = 420 \text{ nm}$  characteristic of  $[\text{Fe}(\text{CN})_6]^{3-}$  and defined as logic **1** and **0** for  $|\Delta\text{Abs}| > 0.1$  or  $|\Delta\text{Abs}| < 0.1$ , respectively. It should be noted that the absorbance measurements for the solutions reacted in the flow device were performed versus the “machinery” solution that contained a constant concentration of  $[\text{Fe}(\text{CN})_6]^{3-}/[\text{Fe}(\text{CN})_6]^{4-}$  that was applied to the reference channel of the spectrophotometer, thus reflecting absorbance difference in the reacting solutions rather than their full absorbance.

Figure 2.18 shows the experimental data obtained upon application of the input signals in 8 different logic combinations. Figure 2.18A, B shows the absorbance changes observed in Output *P* (from the ID gate). In the absence of NADH no absorbance changes were observed, meaning logic **0** value for Output *P*. Each application of NADH (regardless presence or absence of any other species) resulted in the decrease of absorbance at  $\lambda_{\text{max}} = 420 \text{ nm}$ , reflecting the reduction of  $[\text{Fe}(\text{CN})_6]^{3-}$  and resulting in the output logic **1**. Figure 2.18C, D shows the absorbance changes observed in Output *Q* (from the XOR gate). In the absence of NADH and Glc no reactions proceeded and no absorbance changes were observed. The same overall result was observed for the balanced reactions in the presence of both NADH and Glc. Only unbalanced reactions (meaning presence of one of the reacting species, NADH or Glc) resulted in the concentration changes for  $[\text{Fe}(\text{CN})_6]^{3-}$  and corresponding absorbance changes at  $\lambda_{\text{max}} = 420 \text{ nm}$ . This channel represented the XOR gate operation activated by Inputs *A* and *B*. Figure 2.18E, F shows the absorbance changes in Output *R* (from AND-XOR concatenated gates). This channel shows the unchanged absorbance at  $\lambda_{\text{max}} = 420 \text{ nm}$  (meaning the unchanged concentration of  $[\text{Fe}(\text{CN})_6]^{3-}$ ) for input combinations **0, 0, 0** (when no reactions proceed) and **0, 1, 0; 1, 0, 0; 1, 1, 1** (when the reactions are balanced), thus resulting in logic **0** for Output *R*. All other input combinations resulted in the unbalanced reactions and the corresponding optical changes, thus resulting in the logic value **1** for Output *R*. Overall, the obtained experimental data show the output signal pattern, Fig. 2.18, corresponding to the truth table, Fig. 2.15a, characteristic of Peres gate.

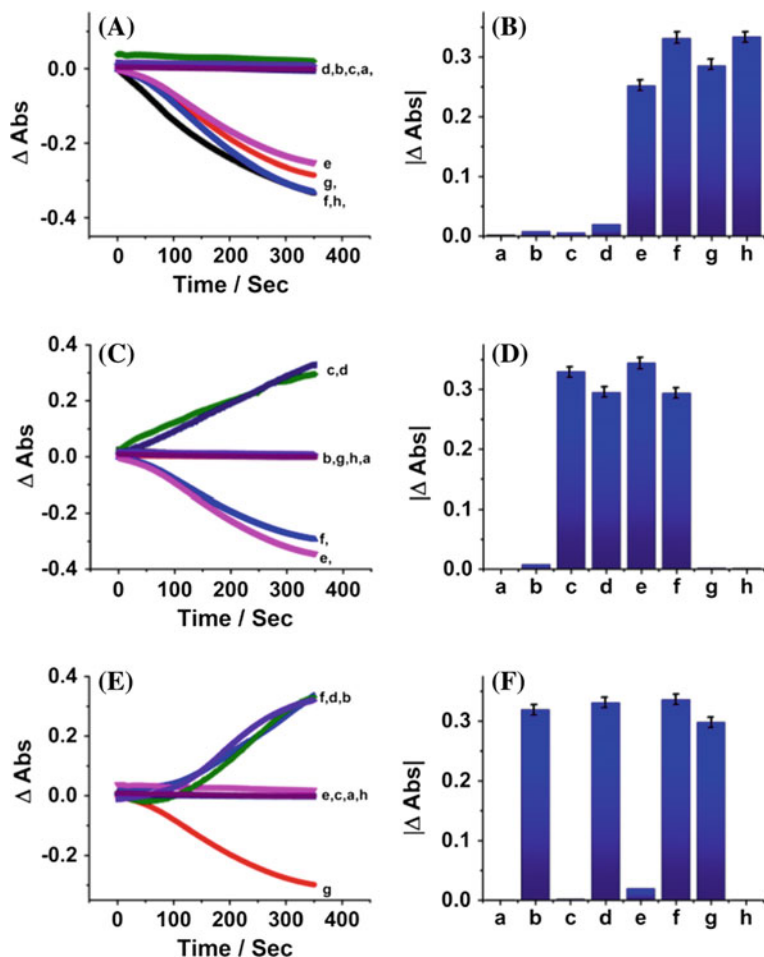


**Fig. 2.18** Optical responses of the Peres gate system to various combinations of the input signals:  $a$  0, 0, 0;  $b$  0, 0, 1;  $c$  0, 1, 0;  $d$  0, 1, 1;  $e$  1, 0, 0;  $f$  1, 0, 1;  $g$  1, 1, 0;  $h$  1, 1, 1. (Note that the logic values are shown for the input signals in the following order:  $A$ ,  $B$ ,  $C$ .) **A**, **B** panels show  $P$  output corresponding to the Identity operation copying  $A$  input signal. **C**, **D** panels show  $Q$  output corresponding to the XOR operation on  $A$  and  $B$  inputs. **E**, **F** panels show  $R$  output corresponding to the AND operation on  $A$  and  $B$  inputs followed by the XOR operation on the output from the AND gate and  $C$  input. **A**, **C** and **E** plots show kinetics of the signal generation. **B**, **D** and **F** bar charts show the signals obtained after 350 s of the flow system operation. All output signals were read at  $\lambda_{\text{max}}$  420 nm. The data shown in the bar-charts are average of three independent experiments (Adapted from Ref. [66] with permission)



## 2.3 Advantages and Disadvantages of the Developed Approach

### 2.3.1 Advantages

Biochemical systems of high complexity composed of many operating enzymes biocatalyzing several reactions cannot be realized in a single solution without compartmentalization of the reacting species similarly to the approach used by Nature in biological cell. Therefore, the approach applied in the present study, where each biocatalytic reaction is running in a separate volume in individual reacting cells and communicating via flow moving from one cell to another, is a good solution for increasing the system complexity. While biocatalytic systems organized in a single solution were limited by maximum 3–4 reaction steps [56, 67] and required extremely complicated optimization [68], the reactions separated in individual cell are much simpler for performance and optimization, thus allowing the increased complexity of the systems. Most important, the modular design with individual flow cells, each modified with one enzyme, allows easy combination of them in various networks for performing different logic operations (AND, XOR, etc.) being parts of the complex information processes, as it is demonstrated in the realized reversible logic gates.

If the signal-processing system needs to have several output signals and when it is organized in one solution, the output signals must have different optical properties being represented by different chemical species. For example, one of the recently reported systems with several inputs and three outputs used individually readable absorbance changes corresponding to NADH and ABTS<sub>ox</sub> ( $\lambda_{\text{max}}$  340 and 420 nm, respectively) and a fluorescence output produced by luciferase-luciferin system in the presence of ATP ( $\lambda_{\text{max}}$  552 nm) [69]. If output signals are read by any other means, for example using redox species analyzed electrochemically, the problem still persists since the produced species should be chemically different to demonstrate different redox potentials that are individually readable by cyclic voltammetry or by any other electrochemical technique. This requirement puts serious limitations on the use of biochemical reactions. The present approach does not have this limitation because the output signals are read from separated channels, thus allowing the outputs to be represented by the same chemical species; for example, NADH can be the output from all logic processes proceeding in parallel in different channels.

Another advantage of the designed biomolecular systems can be found in comparison with the reversible logic systems based on complex synthetic macro-molecules. All-photonic gates activated by light signals and producing light emission as output cannot be easily extended to other chemical information processing steps [43]. On the other hand, the output signals represented by chemical species (e.g., NADH) could be easily connected to the extending information processing steps or even used for chemical actuation processes (e.g., stimulation of drug release) [70, 71].

### 2.3.2 Disadvantages

In electronic realizations of reversible logic gates the input and output signals are represented by electrical potential/current changes. Therefore, the end of one logic gate can be easily connected to the beginning of another. This common property of electronic systems allows assembling reversible logic gates in complex networks for sophisticated computation. In the present chemical realization, the output signals are different by their nature from the input signals. Thus, connecting the logic elements in high hierarchy systems is difficult or even impossible, at least for some of the presently developed systems. This certainly limits the complexity of possible systems. In other words, the chemical extensions of the present logic systems are possible, but connecting the same components to each other is certainly not as trivial as an electronic system.

It should be noted that the developed systems allow *logic reversibility* meaning the possibility to recover the whole set of input signals by analyzing the pattern of the output signals. The biocatalytic reactions cannot run in the opposite directions, thus the physical reversibility is not possible in these systems. Also, the biochemical systems do not have energy saving properties expected theoretically for electronic realization of the reversible computation.

Obviously, the time-scale of the chemical systems operation is in minutes, thus being incomparably longer than that of electronic systems [72]. This makes the use of chemical systems very problematic for realistic computational applications. Even with these drawbacks, the new systems are very interesting for their possible integration with biosensors for logic processing biosensor inputs. Although, this drawback is not as problematic as it may seem, as it could be at least partially resolved if the systems are scaled down to microfluidic devices operating on a shorter time-scale [73].

Overall, it should be noted that the disadvantages briefly discussed above are characteristic of molecular/biomolecular computing systems in general, rather than being specific for the present approach based on the use of flow devices. On the other hand, the advantages of the developed approach clearly demonstrated the possibility of increasing complexity of the information processing systems which is not achievable in a homogeneous system without compartmentalization of reaction steps.

## 2.4 Conclusions and Perspectives

The obtained results demonstrated for the first time information processing in reversible logic gates, such as Feynman gate (CNOT), Double Feynman gate (DFG), Toffoli gate and Peres gate, performed in enzyme-based biocatalytic systems. The first results for CNOT, DFG, Toffoli and Peres gates realized in biocatalytic flow systems [47, 66] are promising for integrating the reversible gates into complex

biomolecular logic networks. The logic processing of biomolecular signals in the reversible mode will be particularly beneficial for biosensing applications that need each combination of the output signals to correspond with a unique pattern of the input signals, thus allowing restoration of the original input values. The application of logically reversible gates for the analysis of biomedically important biomarker signaling for various physiological dysfunctions, similarly to previously reported injury diagnostics [57, 58], are feasible. Technological realization of the information processing systems in flow devices allows for “clocking” (temporal control) as well as spatial separation of the various steps of multistage biochemical processes, thus providing novel options for their sophistication and functional flexibility. The developed approach allows designing other reversible logic gates of higher complexity, including Fredkin gate and other gates with 3-input/3-output and 4-input/4-output compositions [61, 72]. Still technological realization of reversible logic systems with flow networks requires a lot of additional work. Increasing complexity of the interconnected flow networks may result in difficulties, which require fundamental research on biochemical reactions and transport in complex structured systems [74]. Practical use of the systems discussed in this chapter will certainly require transition from the macro-scale flow devices used in the present preliminary study to micro-fluidic lab-on-a-chip devices, allowing their miniaturization and potentially faster response operation.

**Acknowledgments** This work was supported by National Science Foundation (award CBET-1403208).

## Appendix

This section is addressed to the readers interested in technical details of the experimental realization of the reversible logic gates described above.

### *Chemicals and Materials*

Enzymes and their substrates used in the biocatalytic reactions were specified in Sect. 2.2. Results and Discussion (second paragraph).

*Other chemicals used for the immobilization procedure and being components of reacting solutions:* pepsin (E.C. 232.629.3) from porcine gastric mucosa, glutaric dialdehyde, poly(ethyleneimine) solution (PEI) (average  $M_w$  ca. 750,000), 2-amino-2-hydroxymethyl-propane-1,3-diol (Tris-buffer), 2, 2'-azino-bis (3-ethylbenzothiazoline-6-sulfonic acid) diammonium salt (ABTS),  $K_3[Fe(CN)_6]$  and  $K_4[Fe(CN)_6]$ . The chemicals listed above and other standard inorganic/organic reactants were purchased from Sigma-Aldrich and used as supplied. Ultrapure water

(18.2 M $\Omega$ ·cm) from NANOpure Diamond (Barnstead) source was used in all of the experiments.

## ***Instruments and Devices***

Flow cells ( $\mu$ -Slide III 3in1 Flow Kit; ibidi GmbH) were used for the biocatalytic reactions. A Shimadzu UV-2450 UV-Vis spectrophotometer with flow-through quartz cuvettes (1 cm optical pathway) connected to the tubing of the flow device was used for all optical measurements. The reacting solutions were pumped through the flow cells and spectrophotometer cuvettes with the help of a peristaltic pump (Gilson Minipuls 3) connected with polyethylene tubing, 1 mm internal diameter.

## ***Immobilization of Enzymes in the Flow Cells***

Before any experimental data were realized, the flow cells were flushed with concentrated sulfuric acid to remove residual physical adsorption of PEI left on the cell surface from previous experiments. After this initial preparatory step, all subsequent cleanings were conducted with the following method. The flow cells were washed with a minimum of 10 mL of deionized water and then reacted with pepsin solution, 0.5 mg/mL, in 0.1 M phosphate buffer, pH 2.0, for 1 h. Then, the cells were washed with a minimum of 10 mL of deionized water. These cleaning steps aimed at removing remnant enzymes from previous experiments and prepared the cell surface for adsorption of PEI. Then, the flow cells were treated with a PEI solution (2 % v/v) for 1 h and then, thoroughly washed with 5 mL of deionized water, resulting in physical adsorption of PEI on polystyrene and providing the amino groups needed for the enzyme immobilization. Then, the amino-functionalized surface was reacted with glutaric dialdehyde (5 % v/v) for 1 h; after that, the surface was washed with 5 mL of deionized water to remove non-reacted glutaric dialdehyde. The enzyme solutions were reacted with the flow cells and the wells that were activated with glutaric dialdehyde for 1 h and then, the cells were thoroughly washed with Tris-buffer (0.1 M, pH 7.1) to remove non-reacted enzymes from the cells. The following enzyme concentrations were used for preparing the logic gates: (i) Feynman gate: AP ca. 500 units/mL; G6PDH ca. 280 units/mL; LDH ca. 600 units/mL, (ii) Double Feynman gate: GDH ca. 46 units/mL; G6PDH ca. 14 units/mL; LDH ca. 30 units/mL, (iii) Toffoli gate: GDH ca. 140 units/mL; G6PDH ca. 280 units/mL; LDH ca. 340 units/mL; GOx ca. 140 units/mL; HRP ca. 120 units/mL, (iv) Peres gate: GDH ca. 190 units/mL; GOx ca. 665 units/mL; LDH ca. 343 units/mL; HRP ca. 400 units/mL; Diaph ca. 66 units/mL. This procedure resulted in the enzymes covalently bound to the adsorbed PEI through Schiff-base bonds. The flow cell devices with the immobilized enzymes demonstrated reproducible performance for at least two days allowing pumping of the input solu-

tions over long period of time, thus proving stable immobilization of the enzymes and preserving their biocatalytic activity.

### ***Optimization of the Input Concentrations***

The input concentrations were experimentally optimized for the specific enzyme activity in the flow cells. The optimization was aimed at the output signals with the comparable intensity upon application of different combinations of the input signals. Balancing output signals for XOR gates, when optimizing the reversible gates, was particularly important.

The following optimized input concentrations were considered as logic **1** values:

*Feynman gate:* Input A (PNPP + Pyr) 10 mM + 1 mM, respectively, Input B (G6P) 6 mM.

*Double Feynman gate:* Input A (Pyr) 1.46 mM, Input B (G6P) 2.22 mM, Input C (Glc) 0.6 mM.

*Toffoli gate:* Input A (Glc) 0.6 mM, Input B (NAD<sup>+</sup>) 2.75 mM, Input C (Pyr) 1.1 mM.

*Peres gate:* Input A (NADH) 0.02 mM, Input B (Glc) 10 mM, Input C (H<sub>2</sub>O<sub>2</sub>) 0.7 mM.

Logic **0** value for all input signals was defined as the absence of the corresponding chemicals (meaning their zero physical concentration in the background solutions).

### ***Flow Cell Performance and the Output Signal Measurements***

The enzyme-modified flow cells were activated with solutions containing the input signals applied in all possible logic combinations (4 variants for Feynman gate and 8 variants for all other gates). The solutions also included non-variable reacting components which had the same initial concentrations for all combinations of the inputs signals. The solution compositions used for different gate are listed below:

#### ***Feynman gate***

The input signals (represented with PNPP + Pyr and G6P solutions also containing non-variable NADH (0.4 mM) and NAD<sup>+</sup> (10 mM) cofactors) were pumped through the flow system with the volumetric rate of 50  $\mu$ L/min. Optical absorbance measurements were performed for the Identity gate channel (Output *P*) at  $\lambda = 420$  nm characteristic of p-nitrophenol (PNP) and for the XOR gate channel (Output *Q*) at  $\lambda = 340$  nm characteristic of NADH. The reference channel (cuvette) of the spectrophotometer was filled with the background (“machinery”) solution containing NADH (0.4 mM) and NAD<sup>+</sup> (10 mM), thus allowing the absorbance change measurements versus the composition of the background solution.

### *Double Feynman gate*

The input signals (represented with Pyr, G6P and Glc solutions also containing non-variable NADH, 0.4 mM, and NAD<sup>+</sup>, 5.0 mM) were pumped through the flow system with the volumetric rate of 50  $\mu$ L/min. Optical absorbance measurements were performed for the Identity and two XOR gate channels at  $\lambda = 340$  nm characteristic of NADH. The reference channel (cuvette) of the spectrophotometer was filled with the background (“machinery”) solution containing NADH (0.4 mM) and NAD<sup>+</sup> (5.0 mM), thus allowing the absorbance change measurements versus the composition of the background solution.

### *Toffoli gate*

The input signals (represented with Pyr, Glc and NAD<sup>+</sup> solutions also containing non-variable NADH, 0.375 mM, G6P, 0.4 mM, ABTS, 4.0 mM) were pumped through the flow system with the volumetric rate of 50  $\mu$ L/min. Optical absorbance measurements were performed for the GOx/HRP Identity gate at  $\lambda = 415$  nm characteristic of the oxidized form of ABTS (ABTS<sub>ox</sub>), while the G6PDH Identity gate and the AND/XOR gate channels were measured at  $\lambda = 340$  nm characteristic of NADH. The reference channel (cuvette) of the spectrophotometer was filled with the background (“machinery”) solution containing NADH (0.375 mM), G6P (0.4 mM) and ABTS (4.0 mM), thus allowing the absorbance change measurements versus the composition of the background solution.

### *Peres gate*

The input signals (represented with NADH, Glc and H<sub>2</sub>O<sub>2</sub> solutions also containing non-variable K<sub>4</sub>[Fe(CN)<sub>6</sub>] 2.0 mM, K<sub>3</sub>[Fe(CN)<sub>6</sub>] 1.0 mM and Pyr 0.065 mM) were pumped through the flow system with the volumetric rate of 25  $\mu$ L/min. Optical absorbance measurements were performed at  $\lambda = 420$  nm characteristic of K<sub>3</sub>[Fe(CN)<sub>6</sub>]. The reference channel (cuvette) of the spectrophotometer was filled with the background (“machinery”) solution containing K<sub>4</sub>[Fe(CN)<sub>6</sub>] 2.0 mM, K<sub>3</sub>[Fe(CN)<sub>6</sub>] 1.0 mM and Pyr 0.065 mM, thus allowing the absorbance change measurements versus the composition of the background solution.

## References

1. Calude, C.S., Costa, J.F., Dershowitz, N., Freire, E., Rozenberg, G. (eds.): Unconventional Computation. Lecture Notes in Computer Science, vol. 5715. Springer, Berlin (2009)
2. Szacilowski, K.: Infochemistry. Wiley, Chichester (2012)
3. de Silva, A.P.: Molecular Logic-Based Computation. Royal Society of Chemistry, Cambridge (2013)
4. Katz, E. (ed.): Molecular and Supramolecular Information Processing – From Molecular Switches to Unconventional Computing. Wiley-VCH, Weinheim (2012)
5. de Silva, A.P.: Molecular logic and computing. *Nat. Nanotechnol.* **2**, 399–410 (2007)

6. Claussen, J.C., Hildebrandt, N., Susumu, K., Ancona, M.G., Medintz, I.L.: Complex logic functions implemented with quantum dot bionanophotonic circuits. *ACS Appl. Mater. Interfaces* **6**, 3771–3778 (2014)
7. Pischel, U.: Advanced molecular logic with memory function. *Angew. Chem. Int. Ed.* **49**, 1356–1358 (2010)
8. Szacilowski, K.: Digital information processing in molecular systems. *Chem. Rev.* **108**, 3481–3548 (2008)
9. Pischel, U., Andreasson, J., Gust, D., Pais, V.F.: Information processing with molecules - Quo Vadis? *ChemPhysChem* **14**, 28–46 (2013)
10. Katz, E. (ed.): *Biomolecular Computing – From Logic Systems to Smart Sensors and Actuators*. Willey-VCH, Weinheim (2012)
11. Benenson, Y.: Biomolecular computing systems: principles, progress and potential. *Nat. Rev. Genet.* **13**, 455–468 (2012)
12. Alon, U.: *An Introduction to Systems Biology. Design Principles of Biological Circuits*. Chapman & Hall/CRC Press, Boca Raton (2007)
13. Adleman, L.M.: Molecular computation of solutions to combinatorial problems. *Science* **266**, 1021–1024 (1994)
14. Stojanovic, M.N., Stefanovic, D., Rudchenko, S.: Exercises in molecular computing. *Acc. Chem. Res.* **47**, 1845–1852 (2014)
15. Stojanovic, M.N., Stefanovic, D.: Chemistry at a higher level of abstraction. *J. Comput. Theor. Nanosci.* **8**, 434–440 (2011)
16. Ezziene, Z.: DNA computing: Applications and challenges. *Nanotechnology* **17**, R27–R39 (2006)
17. Ashkenasy, G., Dadon, Z., Alesebi, S., Wagner, N., Ashkenasy, N.: Building logic into peptide networks: Bottom-up and top-down. *Isr. J. Chem.* **51**, 106–117 (2011)
18. Unger, R., Moulton, J.: Towards computing with proteins. *Proteins* **63**, 53–64 (2006)
19. Katz, E., Privman, V.: Enzyme-based logic systems for information processing. *Chem. Soc. Rev.* **39**, 1835–1857 (2010)
20. Rinaudo, K., Bleris, L., Maddamsetti, R., Subramanian, S., Weiss, R., Benenson, Y.: A universal RNAi-based logic evaluator that operates in mammalian cells. *Nat. Biotechnol.* **25**, 795–801 (2007)
21. Arugula, M.A., Shroff, N., Katz, E., He, Z.: Molecular AND logic gate based on bacterial anaerobic respiration. *Chem. Commun.* **48**, 10174–10176 (2012)
22. Kahan, M., Gil, B., Adar, R., Shapiro, E.: Towards molecular computers that operate in a biological environment. *Phys. D* **237**, 1165–1172 (2008)
23. Baron, R., Lioubashevski, O., Katz, E., Niazov, T., Willner, I.: Elementary arithmetic operations by enzymes: a model for metabolic pathway based computing. *Angew. Chem. Int. Ed.* **45**, 1572–1576 (2006)
24. Stojanovic, M.N., Stefanovic, D.: Deoxyribozyme-based half-adder. *J. Am. Chem. Soc.* **125**, 6673–6676 (2003)
25. Benenson, Y.: Biocomputing: DNA computes a square root. *Nat. Nanotechnol.* **6**, 465–467 (2011)
26. Pei, R.J., Matamoros, E., Liu, M.H., Stefanovic, D., Stojanovic, M.N.: Training a molecular automaton to play a game. *Nat. Nanotechnol.* **5**, 773–777 (2010)
27. Qian, L., Winfree, E., Bruck, J.: Neural network computation with DNA strand displacement cascades. *Nature* **475**, 368–372 (2011)
28. MacVittie, K., Halámek, J., Privman, V., Katz, E.: A bioinspired associative memory system based on enzymatic cascades. *Chem. Commun.* **49**, 6962–6964 (2013)
29. Privman, V., Katz, E.: Can bio-inspired information processing steps be realized as synthetic biochemical processes? *Phys. Status Solidi A* **212**, 219–228 (2015)
30. Katz, E.: Biocomputing - Tools, aims, perspectives. *Curr. Opin. Biotechnol.* **34**, 202–208 (2015)
31. de Silva, A.P.: Molecular computing - A layer of logic. *Nature* **454**, 417–418 (2008)
32. Benenson, Y.: Biocomputers: from test tubes to live cells. *Mol. Biosyst.* **5**, 675–685 (2009)



33. Pérez-Inestrosa, E., Montenegro, J.-M., Collado, D., Suau, R., Casado, J.: Molecules with multiple light-emissive electronic excited states as a strategy toward molecular reversible logic gates. *J. Phys. Chem. C* **111**, 6904–6909 (2007)
34. Cervera, J., Mafé, S.: Multivalued and reversible logic gates implemented with metallic nanoparticles and organic ligands. *ChemPhysChem* **11**, 1654–1658 (2010)
35. Remón, P., Ferreira, R., Montenegro, J.-M., Suau, R., Perez-Inestrosa, E., Pischel, U.: Reversible molecular logic: a photophysical example of a Feynman gate. *ChemPhysChem* **10**, 2004–2007 (2009)
36. Remón, P., Hammarson, M., Li, S., Kahnt, A., Pischel, U., Andréasson, J.: Molecular implementation of sequential and reversible logic through photochromic energy transfer switching. *Chem. Eur. J.* **17**, 6492–6500 (2011)
37. Sun, W., Xu, C.H., Zhu, Z., Fang, C.J., Yan, C.H.: Chemical-driven reconfigurable arithmetic functionalities within a fluorescent tetrathiafulvalene derivative. *J. Phys. Chem. C* **112**, 16973–16983 (2008)
38. Fratto, B.E., Roby, L.J., Guz, N., Katz, E.: Enzyme-based logic gates switchable between OR, NXOR and NAND Boolean operations realized in a flow system. *Chem. Commun.* **50**, 12043–12046 (2014)
39. Sun, W., Zheng, Y.-R., Xu, C.-H., Fang, C.-J., Yan, C.-H.: Fluorescence-based reconfigurable and resettable molecular arithmetic mode. *J. Phys. Chem. C* **111**, 11706–11711 (2007)
40. Liu, D.B., Chen, W.W., Sun, K., Deng, K., Zhang, W., Wang, Z., Jiang, X.Y.: Resettable, multi-readout logic gates based on controllably reversible aggregation of gold nanoparticles. *Angew. Chem. Int. Ed.* **50**, 4103–4107 (2011)
41. O'Steen, M.R., Cornett, E.M., Kolpashchikov, D.M.: Nuclease-containing media for resettable operation of DNA logic gates. *Chem. Commun.* **51**, 1429–1431 (2015)
42. Semeraro, M., Credi, A.: Multistable self-assembling system with three distinct luminescence outputs: prototype of a bidirectional half-subtractor and reversible logic device. *J. Phys. Chem. C* **114**, 3209–3214 (2010)
43. Andréasson, J., Pischel, U., Straight, S.D., Moore, T.A., Moore, A.L., Gust, D.: All-photonic multifunctional molecular logic device. *J. Am. Chem. Soc.* **133**, 11641–11648 (2011)
44. Orbach, R., Remacle, F., Levine, R.D., Willner, I.: Logic reversibility and thermodynamic irreversibility demonstrated by DNAzyme-based Toffoli and Fredkin logic gates. *Proc. Natl. Acad. USA* **109**, 21228–21233 (2012)
45. Roy, S., Prasad, M.: Novel proposal for all-optical Fredkin logic gate with bacteriorhodopsin-coated microcavity and its applications. *Opt. Eng.* **49**, Article ID 065201 (2010)
46. Klein, J.P., Leete, T.H., Rubin, H.: A biomolecular implementation of logically reversible computation with minimal energy dissipation. *Biosystems* **52**, 15–23 (1999)
47. Moseley, F., Halámek, J., Kramer, F., Poghossian, A., Schöning, M.J., Katz, E.: An enzyme-based reversible CNOT logic gate realized in a flow system. *Analyst* **139**, 1839–1842 (2014)
48. Katz, E., Wang, J., Privman, M., Halámek, J.: Multi-analyte digital enzyme biosensors with built-in Boolean logic. *Anal. Chem.* **84**, 5463–5469 (2012)
49. Wang, J., Katz, E.: Digital biosensors with built-in logic for biomedical applications. *Isr. J. Chem.* **51**, 141–150 (2011)
50. Landauer, R.: Irreversibility and heat generation in the computing process. *IBM J. Res. Develop.* **5**, 261–269 (1961)
51. Toffoli, T.: Physics and computation. *Int. J. Theor. Phys.* **21**, 165–175 (1982)
52. Fredkin, E., Toffoli, T.: Conservative logic. *Int. J. Theor. Phys.* **21**, 219–253 (1982)
53. Takeuchi, N., Yamanashi, Y., Yoshikawa, N.: Reversible logic gate using adiabatic superconducting devices. *Sci. Rep.* **4**, Article ID 6354 (2014)
54. Bennett, C.H.: Logical reversibility of computation. *IBM J. Res. Develop.* **17**, 525–532 (1973)
55. Zhou, J., Arugula, M.A., Halámek, J., Pita, M., Katz, E.: Enzyme-based NAND and NOR logic gates with modular design. *J. Phys. Chem. B* **113**, 16065–16070 (2009)
56. Privman, V., Arugula, M.A., Halámek, J., Pita, M., Katz, E.: Network analysis of biochemical logic for noise reduction and stability: a system of three coupled enzymatic AND gates. *J. Phys. Chem. B* **113**, 5301–5310 (2009)

57. Halámková, L., Halámek, J., Bocharova, V., Wolf, S., Mulier, K.E., Beilman, G., Wang, J., Katz, E.: Analysis of biomarkers characteristic of porcine liver injury - From biomolecular logic gates to animal model. *Analyst* **137**, 1768–1770 (2012)
58. Halámek, J., Windmiller, J.R., Zhou, J., Chuang, M.-C., Santhosh, P., Strack, G., Arugula, M.A., Chinnapareddy, S., Bocharova, V., Wang, J., Katz, E.: Multiplexing of injury codes for the parallel operation of enzyme logic gates. *Analyst* **135**, 2249–2259 (2010)
59. Toepke, M.W., Abhyankar, V.V., Beebe, D.J.: Microfluidic logic gates and timers. *Lab Chip* **7**, 1449–1453 (2007)
60. Scida, K., Li, B.L., Ellington, A.D., Crooks, R.M.: DNA detection using origami paper analytical devices. *Anal. Chem.* **85**, 9713–9720 (2013)
61. Garipelly, R., Madhu Kiran, P., Santhosh Kumar, A.: A Review on reversible logic gates and their implementation. *Int. J. Emerging Technol. Adv. Eng.* **3**, 417–423 (2013)
62. O'Brien, J.L., Pryde, G.J., White, A.G., Ralph, T.C., Branning, D.: Demonstration of an all-optical quantum controlled-NOT gate. *Nature* **426**, 264–267 (2003)
63. Monroe, C., Meekhof, D.M., King, B.E., Itano, W.M., Wineland, D.J.: Demonstration of a fundamental quantum logic gate. *Phys. Rev. Lett.* **75**, 4714–4717 (1995)
64. Siomau, M., Fritzsche, S.: Universal quantum Controlled-NOT gate. *Eur. Phys. J. D* **60**, 417–421 (2010)
65. Privman, V., Zhou, J., Halámek, J., Katz, E.: Realization and properties of biochemical-computing biocatalytic XOR gate based on signal change. *J. Phys. Chem. B* **114**, 13601–13608 (2000)
66. Fratto, B.E., Katz, E.: Reversible logic gates based on enzyme-biocatalyzed reactions and realized in flow cells – Modular approach. *ChemPhysChem* **1**, 1 (2015, in press)
67. Privman, V., Zavalov, O., Halámková, L., Moseley, F., Halámek, J., Katz, E.: Networked enzymatic logic gates with filtering: new theoretical modeling expressions and their experimental application. *J. Phys. Chem. B* **117**, 14928–14939 (2013)
68. Halámek, J., Bocharova, V., Chinnapareddy, S., Windmiller, J.R., Strack, G., Chuang, M.-C., Zhou, J., Santhosh, P., Ramirez, G.V., Arugula, M.A., Wang, J., Katz, E.: Multi-enzyme logic network architectures for assessing injuries: digital processing of biomarkers. *Molec. Biosyst.* **6**, 2554–2560 (2010)
69. Guz, N., Halámek, J., Rusling, J.F., Katz, E.: A biocatalytic cascade with several output signals - Towards biosensors with different levels of confidence. *Anal. Bioanal. Chem.* **406**, 3365–3370 (2014)
70. Mailloux, S., Guz, N., Zakharchenko, A., Minko, S., Katz, E.: Majority and minority gates realized in enzyme-biocatalyzed systems integrated with logic networks and interfaced with bioelectronic systems. *J. Phys. Chem. B* **118**, 6775–6784 (2014)
71. Mailloux, S., Halámek, J., Katz, E.: A model system for targeted drug release triggered by biomolecular signals logically processed through enzyme logic networks. *Analyst* **139**, 982–986 (2014)
72. De Vos, A.: *Reversible Computing: Fundamentals, Quantum Computing, and Applications*. Wiley-VCH, Weinheim (2010)
73. Zhao, Y., Chakrabarty, K.: Digital microfluidic logic gates and their application to built-in self-test of lab-on-chip. *IEEE Trans. Biomed. Circuits Syst.* **4**, 250–262 (2010)
74. Konkoli, Z.: *Phys. Rev. E* **72**, Article ID 011917 (2005)

Advances in Unconventional Computing

Volume 2: Prototypes, Models and Algorithms

Adamatzky, A. (Ed.)

2017, IX, 812 p. 428 illus., 234 illus. in color., Hardcover

ISBN: 978-3-319-33920-7